Chapter 3

MAGNETIC HYSTERESIS MODELING FOR SPICE SIMULATIONS

3.1. Introduction

Magnetic hysteresis is probably one of the most fascinating and complex physical phenomena. While (dynamically) quasi-linear magnetic materials are the basis of many practical applications (linear inductors, power transformer etc.), there exist several examples wherein the exploitation of non-linear magnetic materials is central to obtaining good signal detection performance. An example of such a case is the fluxgate magnetometer that is based on the periodic saturation of a soft-ferromagnetic core [3.1].

Simulations are even more crucial, today, because numerical simulations, finalized to system-level validation and optimization, have become an everyday task. As the number of applications of magnetic materials in the field of power electronic and transducers grows, the need for accurate but simple hysteresis models is becoming very strong.

In the past years, many mathematical hysteresis models have been developed, but unfortunately, few of them can be implemented in SPICE or SPICE-like simulators [3.2]. Among the implementable models, the Jiles-Atherton (JA) model [3.3] is probably the best known and the most used, mainly because it is natively supported by most of the modern SPICE packages [3.4]. Many magnetic materials vendors (mainly in the power-electronics field) include the JA parameters in their product

datasheets [3.5, 3.6]. However, when dealing with some classes of materials, even if the four JA model parameters (or five, depending on the implementation [3.4]) are physically meaningful, they cannot be easily determined from measured data; complex numerical optimization procedures are always necessary. This could be a quite difficult task, in particular for the JA model [3.7]. For this reason the literature offers a large number of papers on the parameter characterization of the JA model, using different soft-computing methodologies or combination thereof [3.8]. Further, much work has been done on the extension and improvement of the original JA model [3.9-3.17]; while most of these attempts are of great value from the physical and methodological point of view, they cannot be easily implemented in SPICE-like simulators because they add parameters and/or differential equations to an already quite complex model. Finally, the JA model suffers to accurately describe some specific hysteresis loop shapes, also when an optimized set of parameters has been found; as an example, it fails to adequately describe the abrupt magnetization curve, typical of soft magnets and of most amorphous ferromagnetic materials. The lack of generality is a common problem in the field of hysteresis models; only strictly geometrical ones, like PWL (Piece-Wise Linear) approximations, suffer less from this drawback (but, again, at the cost of a very large number of parameters to be identified that limits their implementation [3.18]). Amorphous magnetic materials are used as magnetic cores for the realization of fluxgate magnetometers, due to their low coercivity and very sharp hysteresis loop [3.19-3.21]. In this paper, the case of magnetic cores, with abrupt hysteresis loop, to be used in Fluxgate magnetometers are taken into account. A new model is proposed which overcomes the above mentioned limitations.

The main advantages of the proposed model over traditional approaches can be summarized in the following key-points:

1. Easily implementable in any SPICE-like simulator that supports Analog Behavioral Modeling
2. The model is for amorphous materials with abrupt hysteresis loops

3. A small set of parameters (three) has to be identified thus simplifying the modeling procedure
4. If needed, the frequency and the amplitude related behavior of model parameters can be easily obtained.

3.2. The Proposed Core Model

The proposed hysteresis model is a parameterization of the M-H loop already discussed in [3.1]. It consists of a nonlinear first-order differential equation with three parameters (Fig. 3.1):

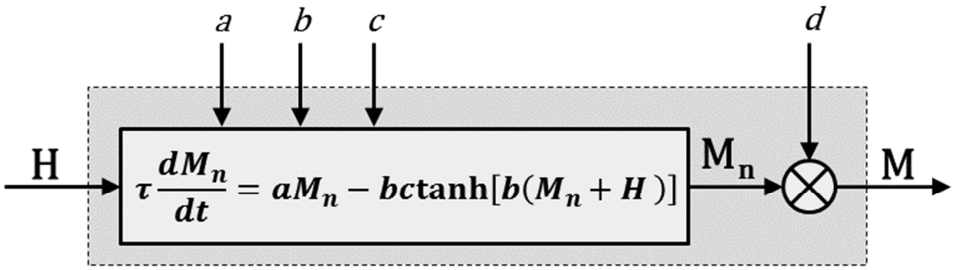

Figure 3.1 - Block diagram schematization of the proposed M-H core model

where M is the core magnetization, Mn is the normalized core magnetization, τ is the system time constant, H is the applied magnetic field intensity, $[a,b,c]$ are three model parameters and d an additional scaling parameter. This model belongs to the "empirical data-fit" class of magnetic hysteresis models [3.2], since it is not strictly physically meaningful. In the following τ will be assumed equal to 1s for the sake of convenience, without compromising the validity of the proposed approach.

The state of the art in the field of fluxgate magnetometer modeling via numerical simulations includes: FEM analysis finalized to the device optimization [3.19, 3.20], SPICE simulations exploiting the JA model [3.21], and numerical hysteresis models starting from standard SPICE components [3.22]. However, the accuracy of these approaches is poor when compared to the experimental results especially when, for simplicity, the hysteretic core has been replaced with a nonlinear, anhysteretic inductor [3.19, 3.20, 3.23].

Here, starting from the *M-H* model just discussed, a complete behavioral model of a RTD fluxgate magnetometer has been developed. It consists of four processing blocks that are briefly described in the following. The main goal of the presented activity is to develop a model which uses the same input/output quantities of the real device: two inputs, the excitation current and the target magnetic field to be measured, and one output, the pick-up voltage at the secondary coil. The latter will allow for the efficient behavioral representation of the real device (fig. 3.3).

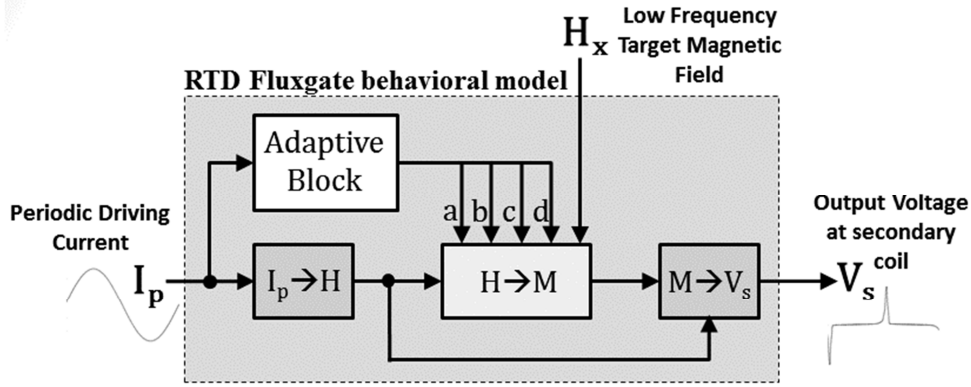

Figure 3.3 - Block diagram schematization of the complete RTD Fluxgate model

3.2.1. The "*Ip→H*" block

The "*Ip→H*" block takes into account the geometry of the primary coil of the magnetometer, implementing the well-known relationship between the current flowing through a solenoid and the resulting axial magnetic field intensity:

$$H = \frac{N_p}{\sqrt{{D_p}^2 + {L_p}^2}} I_p \qquad (1)$$

Using the above equation we are assuming that the excitation field that the magnetic core experiences is equal to the value at the center of the primary coil and this value is constant along the axis. However, given the geometry of the prototype under test, the actual error can be neglected.

3.2.2. The “Adaptive” Block

In order to make the proposed model adaptive to the operating condition (amplitude and frequency of the driving current) an “Adaptive Block” has been implemented. Starting from the processing of the excitation current, it feeds the $H \rightarrow M$ block with the correct set of parameters, by analytical interpolation of the parameter values, extracted from measured data.

3.2.3. The “$H \rightarrow M$” block

The “H→M” block implements the hysteresis model already discussed in section 2. An additional term, Hx, has been introduced, in order to simulate the effects of an applied magnetic field intensity, that is typically DC or slowly varying (much slower than the excitation frequency):

$$\tau \frac{dM}{dt} = aM - bctanh[b(M + H + H_x)] \qquad (2)$$

This allows the numerical estimation of the sensitivity and the full-scale operating range of the magnetometer, given the operating condition. More importantly, in this way it’s possible to observe the behavior of the readout electronics with respect to an applied magnetic field; the optimization of this behavior is one of the aspects of the global performance optimization.

3.2.4. The “$M \rightarrow Vs$” block

The last step in the modeling process is the conversion of the magnetization curve into the output voltage at the secondary coil. This has been implemented by the “$M \rightarrow Vs$” block, which uses the following expression:

$$V_s = -N_s \frac{d\varphi}{dt} = -\frac{N_s \pi {D_s}^2}{4} \frac{dB}{dt} = -\frac{\mu_0 N_s \pi {D_s}^2}{4} \frac{d(H+M)}{dt} \quad (3)$$

It should be borne in mind that equations (1) and (3) are based on geometrical parameters which are known a-priori with a reasonable degree of accuracy and will be not considered during the optimization procedure.

3.3. The Parameters Extraction Procedure

An important aspect to be underlined is that, in the case of Fluxgate magnetometers, the only two quantities that can be directly measured are the driving current at the primary coil, Ip, and the output voltage at the secondary coil, Vs. The excitation magnetic field, H, and the core magnetization, M, must be derived numerically through the fundamental physical expressions including geometrical parameters (eq. (1) and (3)). For the sake of simplicity, the two derived quantities are called *Hmeas* and *Mmeas* in the rest of the paper, keeping in mind that have been indirectly estimated.

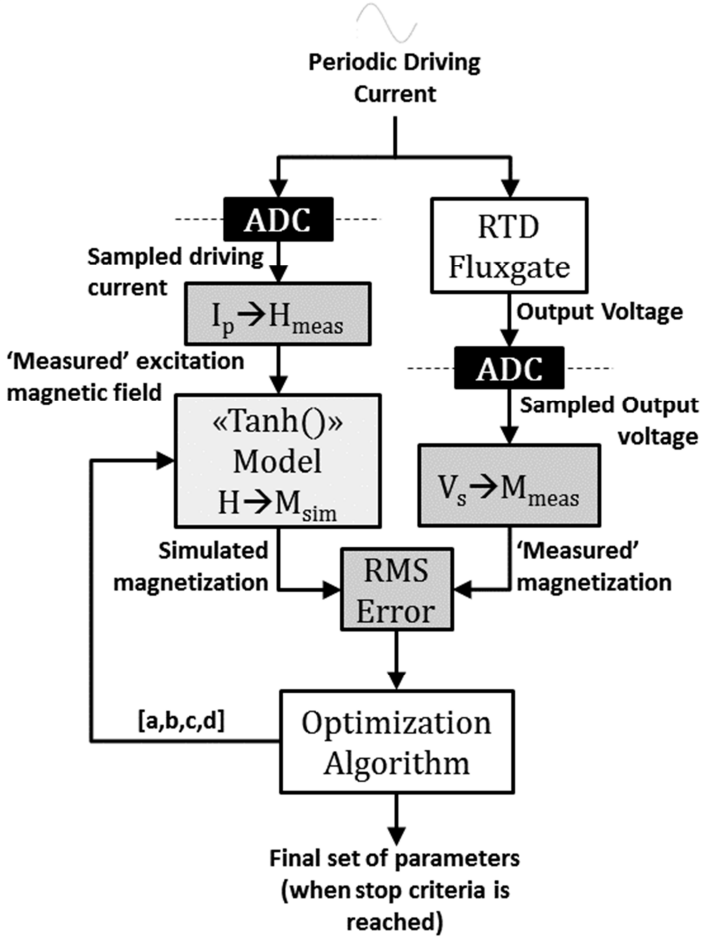

Fig. 3.4 – Flow chart of the parameters extraction procedure

3.3.1. Parameters identification procedure

The parameter extraction procedure can be summarized using the schematization in fig. 3.4.: the periodic driving current, flowing through the primary coil of the magnetometer, is sampled and translated into the corresponding excitation magnetic field (*Hmeas*). The parametric non-linear differential equation is then properly integrated and the corresponding magnetization curve is, therefore, available (*Msim*). This quantity is compared to the measured magnetization, *Mmeas*, (derived from the sampled output voltage *Vs*) and the root mean square error is thus calculated. A suitable optimization algorithm (unconstrained Nelder-Mead simplex process) then calculates the new set of parameters for the next iteration from the elaboration of the error dynamic. This procedure ends when the stop criteria (typically on the error value and/or iteration number) is reached. The d parameter, being a scaling parameter, is not actually given by the optimization algorithm, rather its value is calculated, at the end of each iteration, as the ratio between the measured and simulated magnetization saturation; the optimization problem is, therefore, only 3-dimensional. It has been observed that the optimization algorithm does not require any constraint (for example to prevent negative values or to force similar values for similar operating conditions) and the sensitivity to the initial conditions is extremely low. The latter confirms that complex and time consuming optimization techniques are not needed, in contrast to the JA model.

3.3.2. Development of adaptive models for system parameters

After the optimal set of parameters has been estimated for each operating condition, in the range of interest, models to describe the parameters dependence on the amplitude and the frequency of the driving signal have been studied. In particular, a 2nd order bivariate polynomial function has been used for each parameter:

$$k(f,A) = k_0 + k_1 f^2 + k_2 fA + k_3 A^2 \ , \ k = [a,b,c,d] \quad (4)$$

The *ki* parameters have been identified through a Least-Squares algorithm for bivariate polynomial, that is a one-step procedure, easy to be implemented. Fig. 3.5 shows the interpolation results for the 'a' parameter. The situation for the other three parameters is very similar and, thus, not shown for brevity. The average error within the considered range ([250…750] Hz – [2…12] mApk) is [1.1%, 1.8%, 3.4%, 1.8%] for [*a, b, c, d*] for a second order interpolation.

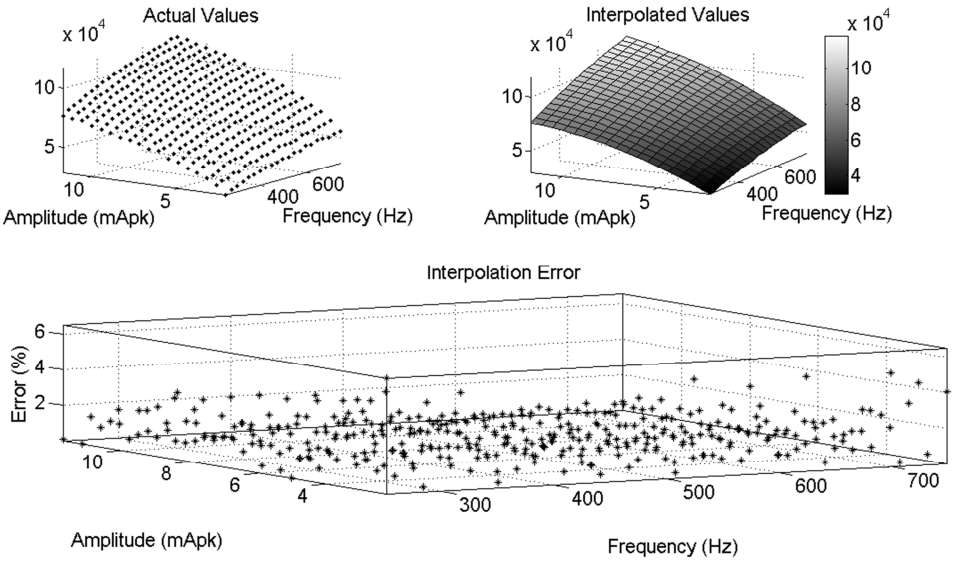

Fig. 3.5 – Interpolation of the 'a' parameter through a 2nd order, bivariate polynomial function. The average error on the considered domain is 1.1%. The other three parameters behaves similarly and are thus not shown.

Adaptive models (4) are of primary importance for the sake of making model (2) adaptive to the operating conditions.

3.3.3. The Graphical User Interface

A Matlab GUI has been developed in order to further simplify the whole processing procedure. It presents a modular architecture, schematized in fig. 3.6. A snapshot of the graphical interface is shown in fig. 3.7.

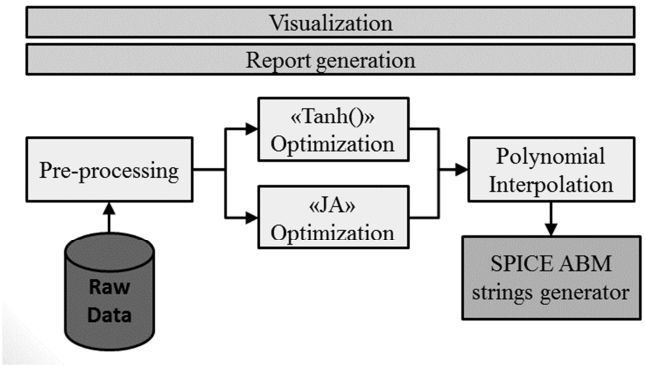

Figure 3.6 – The modular architecture of the developed Matlab GUI

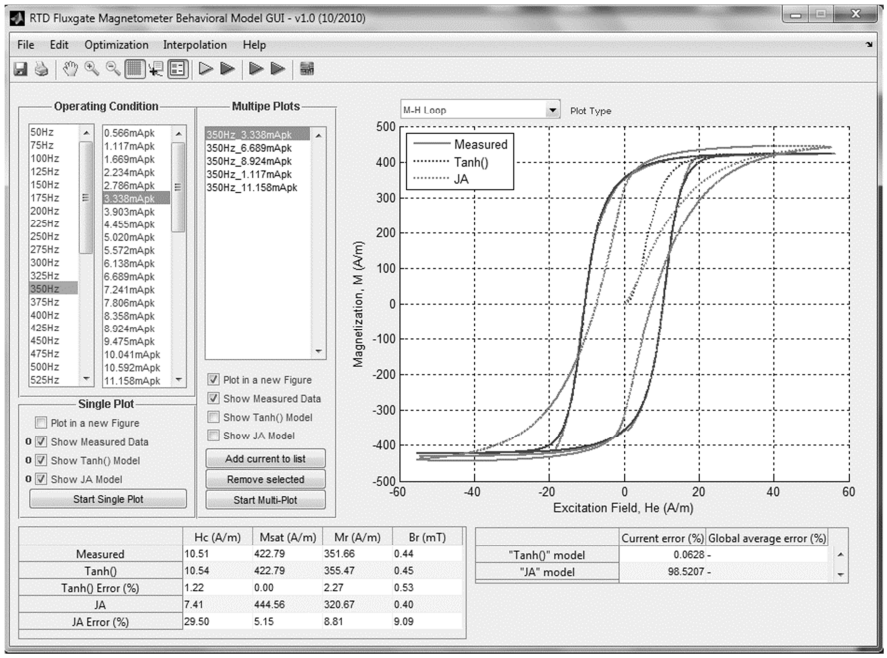

Figure 3.7 – Snapshot of the Matlab GUI

Main features of the developed interface are:

- Smart pre-processing and visualization of the raw data acquired from the magnetometer
- Fully automated parameter extraction procedure
- JA model (with level 2 anhysteretic curve) implementation for comparison purpose
- Adaptive models (by a user-defined order) for the four model parameters
- Generation of Analog Behavioral Modeling (ABM) sources strings, compatible with most of the available SPICE simulators

Thanks to the last feature the software can be regarded as a convenient tool generating the SPICE model, starting from the measured data.

3.4. Model validation in the M-H domain

Simulation results referring to the operating condition of 3mApk @ 325Hz, typical for this kind of magnetometer, are reported in Fig. 3.8. (the JA model, implemented in most SPICE simulators with a level 2 anhysteretic curve [3.4], has been chosen as a benchmark for comparison purposes). As it can be observed, good performance of the proposed model emerges. The estimated RMS errors on the magnetization are 51.6 A/m and 0.04 A/m for the JA and the model (2) respectively. The lack of accuracy of the JA models is also evident in the output voltage waveforms (fig. 3.9).

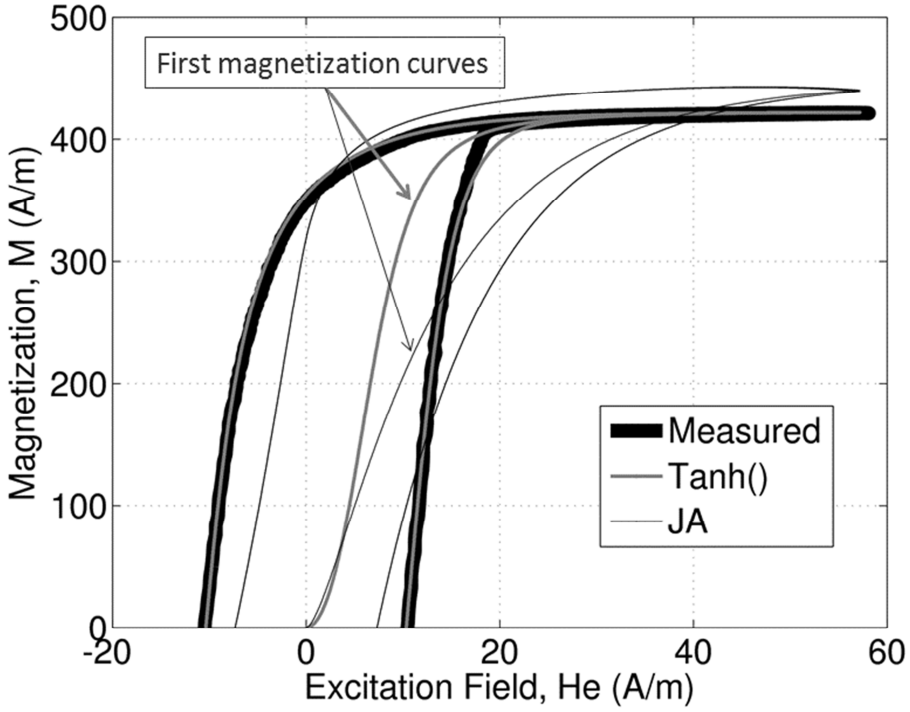

Figure 3.8 – M-H loops for the operating condition of 3mApk @ 325Hz. The first magnetization curve, indicated in the figure by arrows, is missing in the measured loop for the sake of convenience.

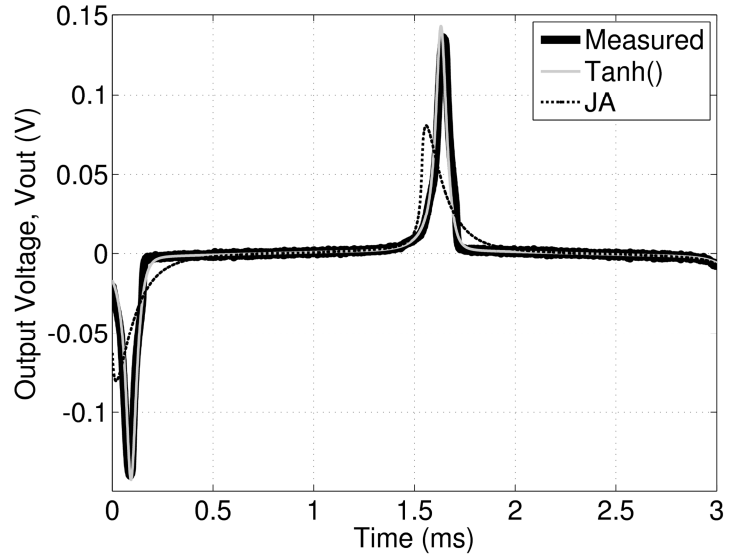

Figure 3.9 – Output voltage at the secondary coil. The lack of accuracy of the JA model produces a poor peak definition.

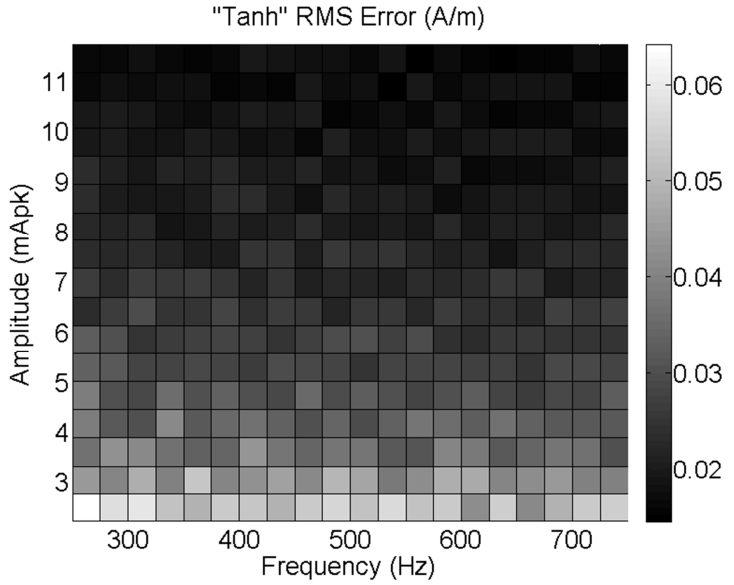

Figure 3.10 – The RMS error on the magnetization estimated by the proposed model on the considered domain. The average value is 0.04 A/m.

The estimated average RMS errors on the magnetization are 0.026 A/m and 47 A/m for the model (2) and the JA model respectively. A detailed plot, showing the error distribution on the whole range of interest, is given in figure 3.10

3.5. Implementation

Multisim (National Instruments) has been chosen, among the available SPICE simulators, because of its strong support for behavioral simulation. Moreover, a tight bi-directional interaction with LabVIEW, thanks to the so-called LabVIEW instruments, increases the capabilities of the software[3.9]. Resembling the schematizations shown in fig. 3.3, the RTD Fluxgate model can be easily implemented as an hierarchical block, by the proper use of ABM (Analog Behavioral Modeling) sources and control block functions: (fig. 3.11):

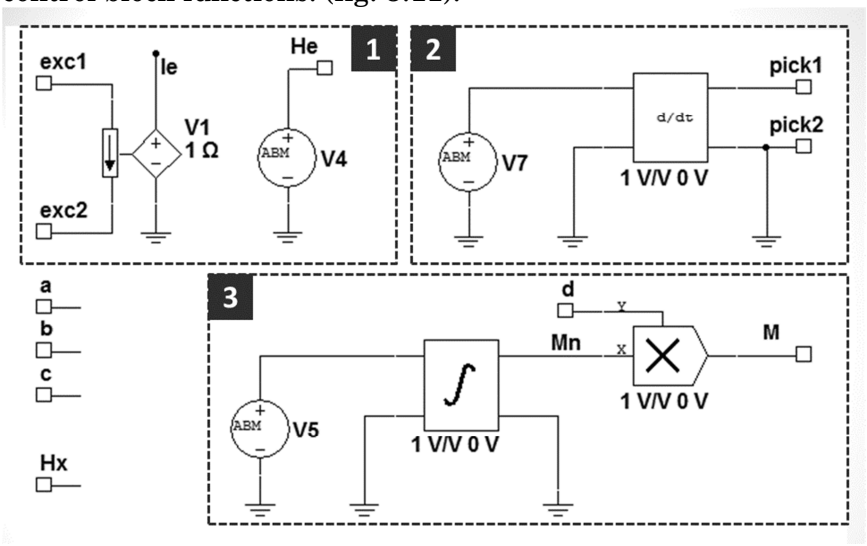

Fig. 3.11 - The three sub-circuits inside the dotted boxes (labeled 1,2 and 3) implement respectively the Ip→H, M→Vs and H→M blocks. Equations (1), (2) and (3) are implemented in the definition of the three ABM sources, V4, V5 and V7.

In order to demonstrate the feasibility of the proposed approach, the magnetometer has been simulated together with its excitation, conditioning and readout circuit (fig. 3.12):

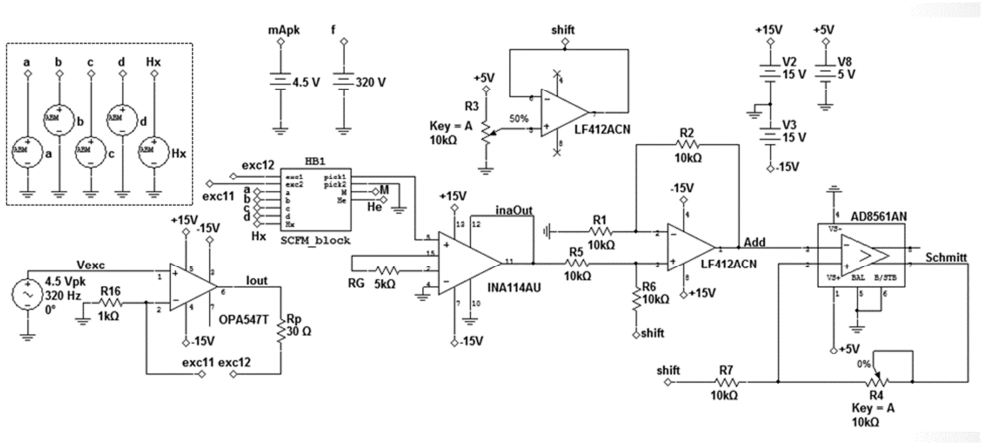

Fig. 3.12 – Snapshot of the Multisim Schematic implementing a typical operating circuit. The four interpolating function (eq. (4)) are implemented in the corresponding ABM sources at top-left. The "HB1" block encloses the model implementation, as shown in fig. 3.11

The magnetometer model appears as a hierarchical block and, thus, behaves like a normal SPICE schematic component. The four ABM sources on the top-left implement the four interpolating functions for each parameter (see eq. (4)); strings for these sources are supplied directly by the GUI through a "cut and paste" action. The actual operating condition, in this simple example, is fixed off-line by setting the value of the two DC power sources *V(f)* and *V(mApk)*. The whole circuit can be summarized as follows: the first stage is a voltage-to-current converter that produces the driving current that is forced through the primary coil; the output voltage of the magnetometer is amplified and level-shifted in order to adapt the levels to a TTL Schmidt Trigger, which produces a square waveform whose duty cycle is related to the *RTD* (Residence Times Difference) and therefore to the value of the target magnetic field (that can be set, in the example shown, by changing the value of the related DC power sources).

In fig. 13 we present a snapshot of the Multisim output window, showing the simulated output voltage and the attendant Schmidt Trigger output. The applied magnetic field starts from zero and then reach linearly the value of 70μT at 20ms. The resulting asymmetry of the time position of the spikes in the output voltage and the corresponding change in the duty cycle of the trigger output show that the model reacts to a simulated target field, as expected. Fig. 14 shows simulated M-H loops at different frequencies ([250, 350, 450, 550, 650] Hz); the inner loops corresponds to lower frequencies.

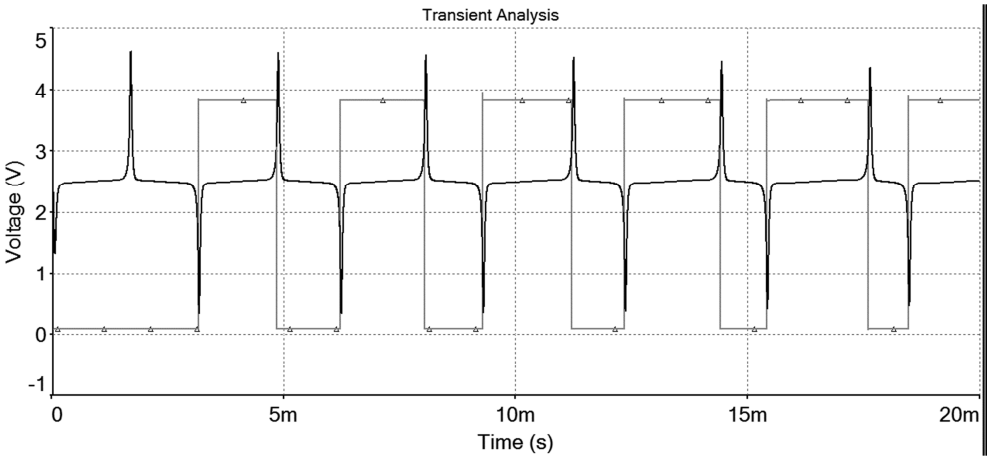

Fig. 3.13 – Multisim simulation results for the operating condition of 4.5mApk @ 350 Hz with a linear ramp applied target field (0μT at 0ms, 70 μT at 20 ms). The black waveform is the output voltage of the magnetometer, after the amplification and level-shift stages. The square waveform is the output of the Schmidt trigger whose duty cycle increases as the target field grows.

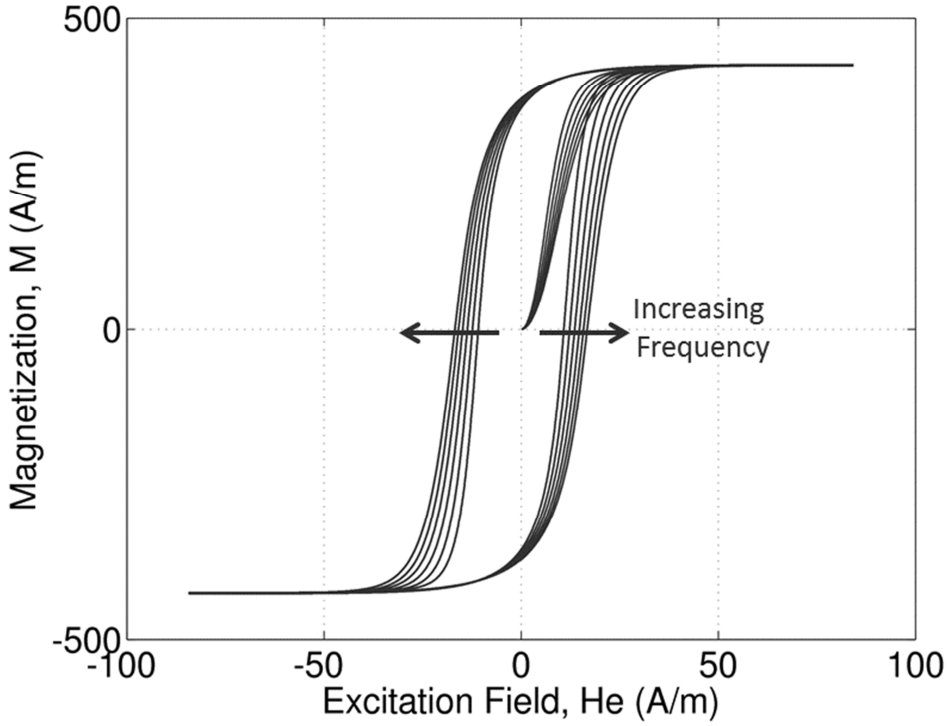

Fig. 3.14 – SPICE simulated M-H loops for 3 mApk @ [25, 350, 450, 550, 650] Hz.

3.6. CCFM SPICE simulation

Starting from the model for the single core magnetometer, discussed in the previous sections, it is possible to simulate the CCFM together with its excitation, conditioning and readout circuit (Fig. 3.15):

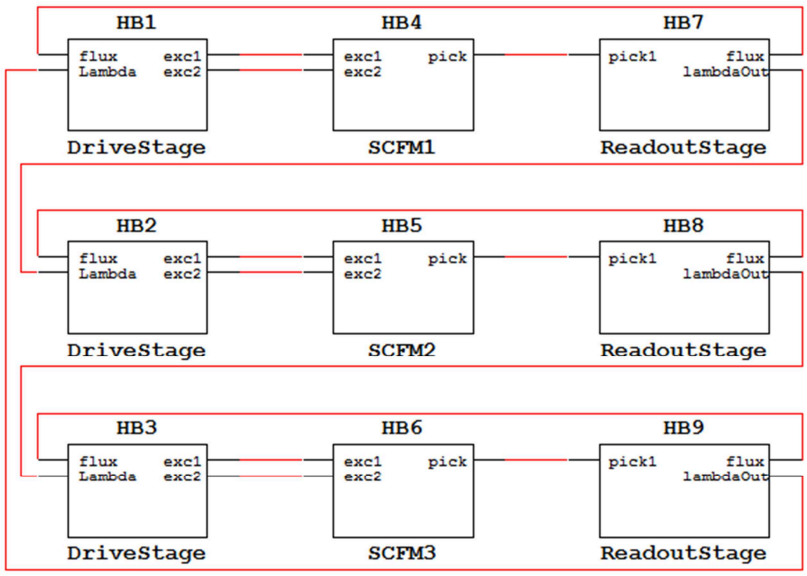

Fig. 3.15 – Snapshot of the NI Multisim schematic window implementing the CCFM model.

The whole circuit can be summarized as follows: the first stage (DriveStage) is a voltage-to-current converter that produces the driving current that is forced through the primary coil; the output voltage of the magnetometer is amplified, integrated and suitably filtered in order to produce a voltage proportional to the core magnetization (ReadoutStage); this signal represent the input of the next element in the ring.

In fig. 16 we report a snapshot of the Multisim output window, showing the simulated output voltage for the three elements. The system exhibits the characteristic oscillating behavior that can be exploited to quantify an external magnetic field, as previously discussed. In fig.

3.17 the simulated calibration curve (RTD variation versus the applied target magnetic field) is shown at different coupling strength.

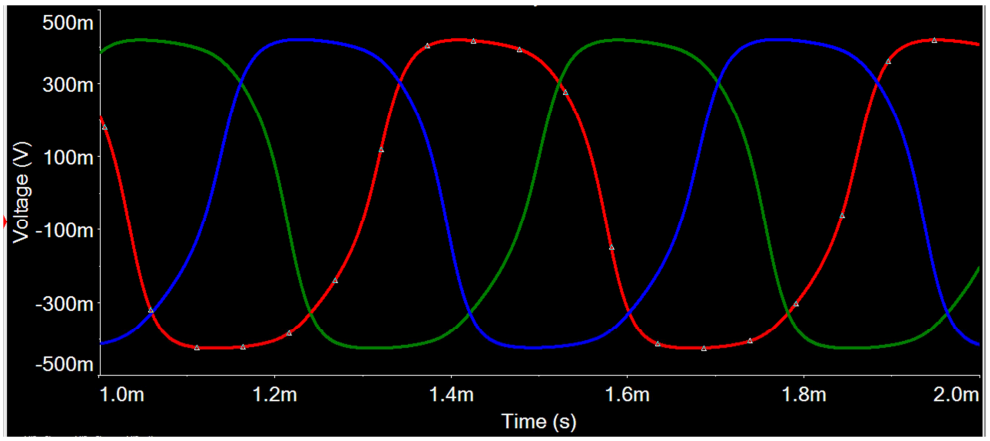

Fig. 3.16 – Snapshot of the NI Multisim output window. The three waveform correspond to the output signals of the three elements that build up the CCFM.

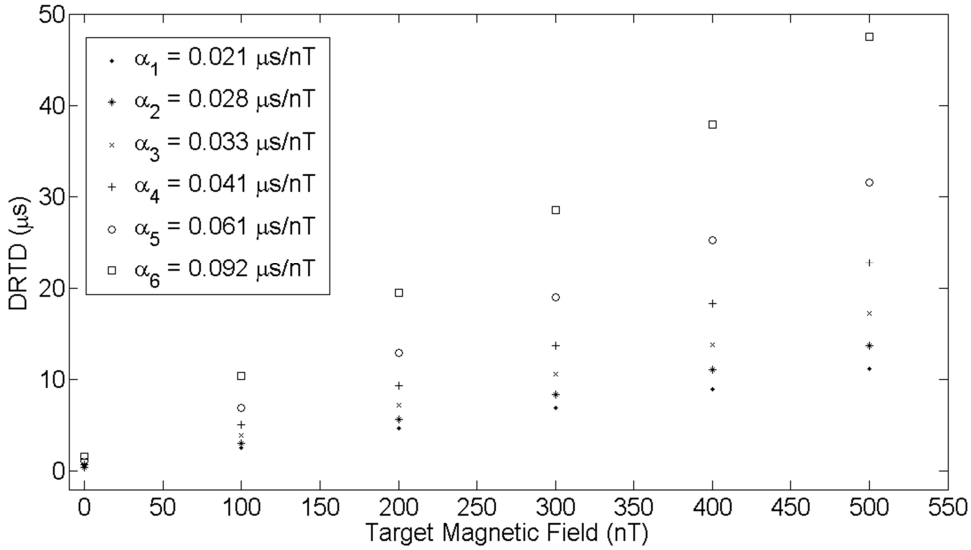

Fig. 3.17 – Simulated calibration curves for different values of the coupling constant, •. The higher the coupling strength, the lower the sensitivity, •, as expected.

3.7. Conclusions

A new SPICE model of magnetic hysteresis has been presented which is particularly convenient in the case of abrupt hysteresis loops. The M-H loop model has been exploited to implement a complete RTD Fluxgate behavioral model, targeted for SPICE simulations, as a case of study. This overcomes the limitations of the already available approaches (e.g. the Jiles-Atherton model implemented in different SPICE packages, used for the sake of comparison). The simplicity and the accuracy of the proposed solution makes the developed methodology suitable for system level numerical simulations, finalized to the system design and optimization.

REFERENCES

[3.1] B. Ando, S. Baglio, A.R. Bulsara, V. Sacco, RTD fluxgate: a low-power nonlinear device to sense weak magnetic fields, Instrumentation & Measurement Magazine, IEEE, 8 (2005) 64-73.
[3.2] M.D. Takach, P.O. Lauritzen, Survey of magnetic core models, in: Applied Power Electronics Conference and Exposition, 1995. APEC '95. Conference Proceedings 1995., Tenth Annual, 1995, pp. 560-566 vol.562.
[3.3] D.C. Jiles, D.L. Atherton, Theory of ferromagnetic hysteresis, Journal of Magnetism and Magnetic Materials, 61 (1986) 48-60.
[3.4] A. Maxim, D. Andreu, J. Boucher, A novel behavioral method of SPICE macromodeling of magnetic components including the temperature and frequency dependencies, in: Applied Power Electronics Conference and Exposition, 1998. APEC '98. Conference Proceedings 1998., Thirteenth Annual, 1998, pp. 393-399 vol.391.
[3.5] J. Izydorczyk, Simulation of ferrites by SPICE, in: Circuit Theory and Design, 2005. Proceedings of the 2005 European Conference on, 2005, pp. I/43-I/46 vol. 41.
[3.6] J. Izydorczyk, Simulation of soft magnetic materials by SPICE, in: Electrotechnical Conference, 2006. MELECON 2006. IEEE Mediterranean, 2006, pp. 141-144.
[3.7] D. Lederer, H. Igarashi, A. Kost, T. Honma, On the parameter identification and application of the Jiles-Atherton hysteresis model for numerical modelling of measured characteristics, Magnetics, IEEE Transactions on, 35 (1999) 1211-1214.
[3.8] M. Toman, G. Stumberger, D. Dolinar, Parameter Identification of the Jiles–Atherton Hysteresis Model Using Differential Evolution, Magnetics, IEEE Transactions on, 44 (2008) 1098-1101.
[3.9] L. Huiqi, L. Qingfeng, X. Xiao-bang, L. Tiebing, L. Lin, A modified method for jiles-atherton hysteresis model and its application in numerical simulation of devices involving magnetic materials, in: Electromagnetic Field Computation (CEFC), 2010 14th Biennial IEEE Conference on, 2010, pp. 1-1.
[3.10] M.V.F. da Luz, J.V. Leite, A. Benabou, N. Sadowski, Three-Phase Transformer Modeling Using a Vector Hysteresis Model and Including

the Eddy Current and the Anomalous Losses, Magnetics, IEEE Transactions on, 46 (2010) 3201-3204.
[3.11] A. Ladjimi, M.R. Mekideche, Model for the behavior of magnetic materials hysteretic taking into account the temperature, in: Systems, Signals and Devices, 2009. SSD '09. 6th International Multi-Conference on, 2009, pp. 1-6.
[3.12] A. Raghunathan, Y. Melikhov, J.E. Snyder, D.C. Jiles, Modeling the Temperature Dependence of Hysteresis Based on Jiles–Atherton Theory, Magnetics, IEEE Transactions on, 45 (2009) 3954-3957.
[3.13] E. Etien, D. Halbert, T. Poinot, Improved Jiles–Atherton Model for Least Square Identification Using Sensitivity Function Normalization, Magnetics, IEEE Transactions on, 44 (2008) 1721-1727.
[3.14] H. Hauser, Y. Melikhov, D.C. Jiles, Including effects of microstructure and anisotropy in theoretical models describing hysteresis of ferromagnetic materials, Applied Physics Letters, 91 (2007) 172512-172512-172513.
[3.15] P.D. Dimitropoulos, G.I. Stamoulis, E. Hristoforou, A 3-D hybrid Jiles-Atherton/Stoner-Wohlfarth magnetic hysteresis model for inductive sensors and actuators, Sensors Journal, IEEE, 6 (2006) 721-736.
[3.16] Z. Wlodarski, The Jiles-Atherton model with variable pinning parameter, Magnetics, IEEE Transactions on, 39 (2003) 1990-1992.
[3.17] K.H. Carpenter, A differential equation approach to minor loops in the Jiles-Atherton hysteresis model, Magnetics, IEEE Transactions on, 27 (1991) 4404-4406.
[3.18] S. Cincotti, Approximation properties of a PWL circuit model of hysteresis, Physica B: Condensed Matter, 275 (2000) 216-222.
[3.19] A. Baschirotto, E. Dallago, P. Malcovati, M. Marchesi, G. Venchi, From a PCB Fluxgate to an integrated micro Fluxgate magnetic sensor, in: Instrumentation and Measurement Technology Conference, 2005. IMTC 2005. Proceedings of the IEEE, 2005, pp. 1756-1760.
[3.20] N. Sharafi, M.A. Nekoui, Analyzing optimization of fluxgate sensor, in: Electronic Design, 2008. ICED 2008. International Conference on, 2008, pp. 1-4.

[3.21] B.-O. Moldovanu, C. Moldovanu, A. Moldovanu, Computer simulation of the transient behavior of a fluxgate magnetometric circuit, Journal of Magnetism and Magnetic Materials, 157-158 (1996) 565-566.
[3.22] S. Gupta, C.H. Ahn, J. Park, II, Electromagnetic modeling and harmonic analysis of micro-machined ring-type magnetic fluxgate sensor using SPICE, in: Sensors, 2003. Proceedings of IEEE, 2003, pp. 622-625 Vol.621.
[3.23] H. Trujillo, J. Cruz, M. Rivero, M. Barrios, Analysis of the fluxgate response through a simple spice model, Sensors and Actuators A: Physical, 75 (1999) 1-7.